A FIRST REPORT ON SINTERING DIAGRAMS*

M. F. ASHBY†

Six or more *distinguishable mechanisms* contribute to the sintering of an aggregate of particles—even in the absence of applied stresses. Diagrams can be constructed which identify, at a given temperature, particle size and neck size, the *dominant mechanism*, and show the *rate of sintering* that all the mechanisms, acting together, produce.

This paper describes the construction of two forms of these diagrams, and illustrates their use in interpreting sintering experiments and in solving practical sintering problems for metals and ceramics.

DIAGRAMMES DE FRITTAGE (PREMIER ARTICLE)

Six *mécanismes distincts*, ou plus, contribuent au frittage d'un aggrégat de particules—même en l'absence de constraintes appliquées. On peut construire des diagrammes qui donnent, à une température donnée, la taille des particules, la taille des cols, le *mécanisme dominant*, et mettent en évidence la *vitesse de frittage* produite par tous les mécanismes agissant ensemble. Cet article décrit la construction de ces diagrammes (sous deux présentations) et illustre leur utilisation pour interpréter les expériences de frittage et pour résoudre les problèmes pratiques de frittage des métaux et des céramiques.

EIN ERSTER BERICHT ÜBER SINTERDIAGRAMME

Sechs oder mehr *unterscheidbare Mechanismen* tragen zum Sintern von Teilchen bei—auch in Abwesenheit einer äußeren Belastung. Es können Diagramme konstruiert werden, mit deren Hilfe man bei vorgegebener Temperatur, Teilchengröße und Sinterhalsgröße den *dominierenden Mechanismus* identifizieren kann und die die Sintergeschwindigkeit zeigen, die sich aufgrund aller wirkenden Mechanismen ergibt.

In der vorliegenden Arbeit wird die Konstruktion von zwei Diagrammformen beschrieben und deren Verwendung zur Interpretation von Sinterexperimenten und zur Lösung praktischer Probleme beim Sintern von Metallen und Keramik erläutert.

1. INTRODUCTION

When a powder aggregate is sintered, necks form between the powder particles, and the aggregate may increase in density. Even in a pure, one-component system (pure silver, for instance) at least *six distinguishable mechanisms* contribute to neck growth and to densification. Most of these involve the diffusive transport of matter to the growing neck; Fig. 1 shows some of the possible diffusion paths.

Certain two-component systems (alloys, for example) are made more complicated by having two diffusing species which move at unequal rates; others (ceramics, for instance) have diffusion coefficients which may vary strongly with deviations from stoichiometry and with trace levels of impurity. The application of a stress or pressure further complicates sintering by introducing new mechanisms, and by accelerating certain of the old ones.

This report considers a relatively simple class of problems: the sintering, in the absence of applied stress, of pure one-component systems, and pure stoichiometric compounds. Even then, the process is a complicated one. The six mechanisms‡ illustrated in Fig. 1 have a common driving force: it is the reduction in the surface area, and thus surface free-energy of the system. They are distinguished by the diffusive path involved, and by the source from which matter is drawn, and the sink to which it flows. The table lists these in order.

TABLE 1

Mechanism No.	Transport path	Source of matter**	Sink of matter**
1	Surface diffusion	Surface	Neck
2	Lattice diffusion	Surface	Neck
3	Vapor transport	Surface	Neck
4	Boundary diffusion	Grain boundary	Neck
5	Lattice diffusion	Grain boundary	Neck
6	Lattice diffusion	Dislocations	Neck

** Sintering problems can be formulated in terms either of the flow of matter, or of the counterflow of vacancies. It is more convenient to focus on the flow of matter.

All of these—and others discussed below—contribute simultaneously to *neck growth:* the neck growth-rate or sintering rate, (dx/dt), is the sum of the six (or more) contributions. Only certain of them lead to *densification:* the rate at which particle centers approach each other, (dy/dt), is non-zero only when matter is removed from the grain boundary which separates two particles (mechanism 4 and 5) or from dislocations within the neck region (mechanism 6). If this boundary and these dislocations were removed, or prevented from acting as sinks for point defects, densification would cease, although neck growth might continue.

‡ Most of these are listed in a recent review by Thummler and Thoma,[1] and in papers by Wilson and Shewmon,[2] and Coble,[3] though no one list includes them all.
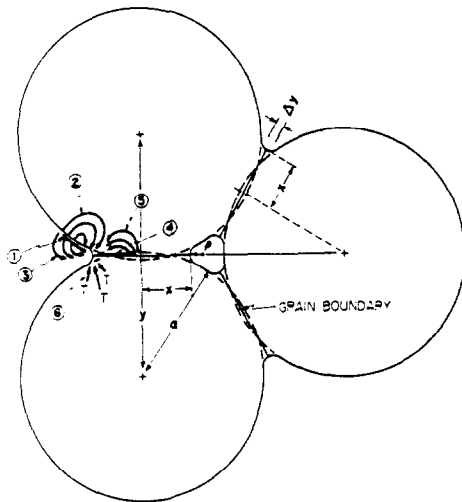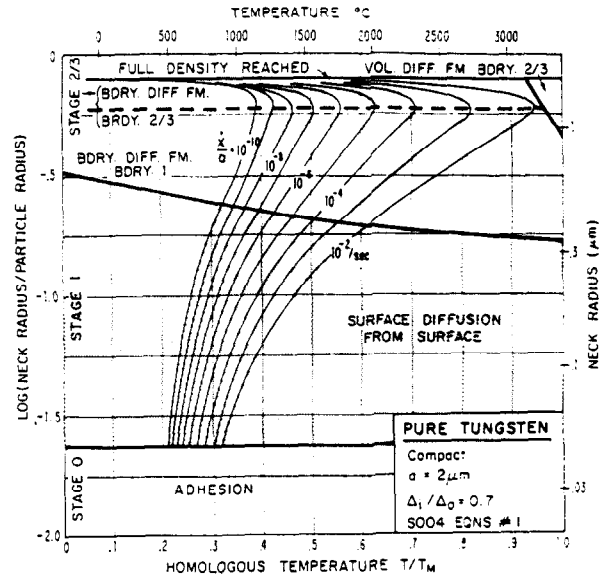
FIG. 1. Six alternative paths which permit diffusion-controlled sintering. All lead to neck growth. Only paths 4–6 cause the particle centers to translate together, and so permit densification.

(a)

(b)

FIG. 2. (a) A sintering-rate diagram for tungsten. The *fields* indicate the dominant mechanism. In an unshaded field the dominant mechanism causes both neck-growth and densification; in a shaded field, only neck growth. The contours are lines of *constant normalized sintering rate*, $\dot{x}/a$; (b) A sintering-time diagram. It is identical with Fig. 2(a), but for the contours, which are now lines of *constant time, t*. This shows the neck size after a given time–temperature treatment.
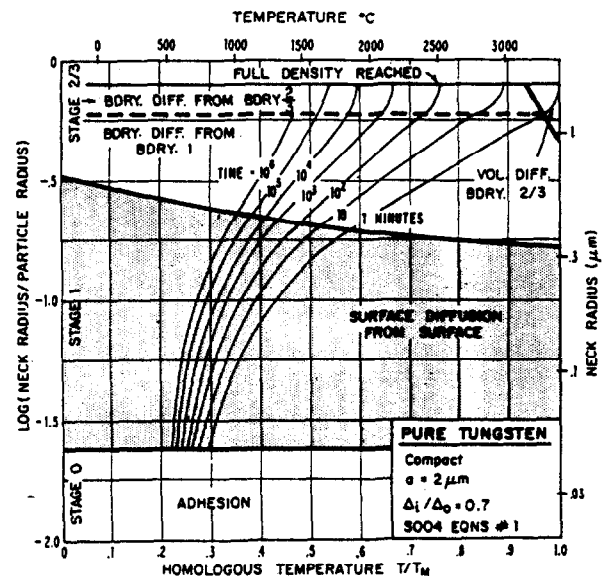
If a powder aggregate is heated at a given temperature, will it densify? What is the neck growth-rate? What is the neck size after a given time? Which of the six or more mechanisms is the dominant one? How can one devise a time–temperature schedule which will lead to maximum density or maximum porosity? These questions have often caused difficulty, because the sintering rate is the sum of several components, not all of which contribute to densification.

One way to answer them is presented in this report. It involves the construction of *sintering diagrams*: diagrams which show for a given temperature and neck size, the dominant mechanism of sintering, and the net rate of neck-growth or densification.

Two forms such diagrams can take are shown in Fig. 2. They describe the sintering of an aggregate of tungsten particles with a radius of 2 μm. The axes are *homologous temperature*, T/T_M, (where T_M is the melting point) and *normalized neck radius*, x/a, (where x is the radius of the disc of contact of two particles, and a is the particle radius). The space defined by these axes is divided into *fields*. Within a field, a single sintering mechanism is dominant: it contributes most to neck growth. The largest field in Fig. 2, for example, is that corresponding to mechanism (1): within this field, surface diffusion of matter from sources on the pore surface is dominant. Superimposed on the fields of Fig. 2(a) are *contours of constant sintering rate*: they show, for a given temperature and neck size, how fast the neck is growing. Figure 2(b) is a more useful version of the

diagram; here the contours are of *constant sintering time*: they show the neck size after a given time.

Diagrams like these are described more fully below. They give the *rate*, and identify the *mechanism* of sintering at a given temperature. As well as their use in designing and interpreting experiments, the diagrams have potential application to practical sintering problems. The unshaded fields describe

mechanisms which lead to densification: if a dense compact is desired, sintering should be performed in an unshaded field. Conversely the maximum porosity is retained if the aggregate is sintered in a shaded field, as far as possible from the boundary with the unshaded ones.

Such diagrams are constructed from *rate-equations*: equations which describe the contribution of each participating mechanism to the neck growth-rate or the densification rate. The next section describes the equations used for this report. I have attempted to select from the literature, or derive where necessary, equations which best combine simplicity with a sufficient level of accuracy. Exhaustive reference to their history and derivation would be out of place; instead, I simply refer to the appropriate review or paper, or indicate the method of derivation.

The diagrams shown in this report are based on two assumptions: that the sintering occurs in the absence of an applied stress or pressure, and that the pores contain no gas other than the vapor of the material being sintered. Diagrams can be constructed which show the effect of pore pressure and of external pressure or stress on sintering, but they will not be described here.

2. RATE EQUATIONS AND THE STAGES OF SINTERING

2.1 Stages of sintering

It is conventional[1] to think of sintering as occurring in *three sequential stages*. Stage 1 is the early stage of neck growth: the individual powder particles are still distinguishable. Stage 2 is the intermediate stage: the necks are now quite large, and the pores are roughly cylindrical. By the time the final stage—stage 3—is reached, the pores are isolated and spherical.

The appropriate rate equation for a mechanism depends on the stage which sintering has reached. In the treatment described below we include a new stage—stage 0—which describes the instantaneous neck-formation which interatomic forces cause when powder particles are placed in contact. The next stage—stage 1—is treated as distinct, with its own rate equations. But we link stages 2 and 3 together, using a single set of rate equations to describe both. Though an approximation, it is adequate for the level of precision aimed at here.

This level of precision is low. The equations listed below are, at best, first approximations. It is true that many of the features of the diagrams we construct from them depend on the *ratio* of rates (not their absolute magnitudes), when many of the approximations cancel. And the scales of the dia-

grams are coarse: an error of a factor or two either way in one rate does not change them much. But the reader is cautioned not to regard the equations as exact, or to attribute too much precision to the diagrams based on them.

The symbols used in the remainder of this section have the following meanings:

a	particle radius
x	radius of disc of contact of two particles
x_f	the final value of x when 100 per cent density has been reached
ρ, ρ_1, ρ_2	radius of curvature of the neck
K_1, K_2, K_3	curvature differences which drive diffusive fluxes
D_s	surface diffusion coefficient
D_v	lattice diffusion coefficient
D_B	grain boundary diffusion coefficient
D_G	diffusion coefficient in the gas phase
δ_s	effective surface thickness
δ_B	effective grain boundary thickness
P_v	vapor pressure $[P_v = P_0 \exp - (Q_{vap}/kT)]$
γ_s	surface free energy
γ_B	grain boundary free energy
Ω	atom or molecular volume
k	Boltzmann's constant (1.38×10^{-16} ergs/K; 1.38×10^{-23} J/K)
T	absolute temperature (K)
T_M	melting temperature (K)
F	$\gamma_s\Omega/kT$ (typically of magnitude 10^{-8} cm)
f	volume fraction of pores
Δ_0	theoretical density
Δ_i	initial density of powder compact
μ	shear modulus
b	Burgers vector of dislocations, or the atomic or molecular diameter
N	dislocation density
c	velocity of sound (taken as 10^5 cm/sec; 10^3 m/sec).

To perform the calculation described below, numerical values for these quantities must be known. In addition to the quantities which vary rapidly with temperature $(D_v D_s D_B D_G P_v)$, an explicit temperature dependence of μ and of γ was included. That of quantities which scale as the lattice parameter $(a, X, \rho, \delta_s, \delta_B, \Omega, \Delta, b)$ was considered to be too small to justify including it.

2.2 The driving force: Surface curvature

In the absence of pressure (or stress), sintering is driven by surface curvature—or rather, by the *difference* in surface curvature between sources and

sinks. This driving force differs for different diffusion paths; and, for a given diffusion path, it can depend on the configuration and geometry of the sintering particles.

The exact calculation of the curvature differences which drive sintering involves difficult geometry, and the solution of time-dependent diffusion equations [see. e.g. Ref. (4)]. Our aim, however, is to display the broad picture of sintering as a whole; clarity and adequate rigor are retained by taking simple expressions for the curvature difference, and adjusting them (when necessary) to give physically obvious asymptotic limits.

Sintering of a row of spheres. Consider first a geometry commonly used in laboratory studies of sintering: a row of spheres in contact†. Figure 3 shows two of them. The broken lines indicate successive position of the growing neck; its radius of curvature is ρ. For simplicity, assume that the driving force goes to zero when the last broken line is reached, that is, when the row of spheres has become a cylinder. (This is not strictly true, but is adequate for all practical purposes.) During the early stages of sintering, the curvature difference for diffusion from a surface source (mechanisms 1–3) is obviously

$$K = \left(\frac{1}{\rho} - \frac{1}{x}\right) + \frac{2}{a} \qquad (1)$$

where, by simple geometry, $\rho = [x^2/2(a - x)]$ (see, e.g. Kuczynski[5]). But this does not go to zero at $x = a$. To make it do so, we multiply the expression by $[1 - (x/a)]$, giving‡

$$K_1 = \left(\frac{1}{\rho} - \frac{1}{x} + \frac{2}{a}\right)\left(1 - \frac{x}{a}\right). \qquad (2)$$

$$(K_1 \geq 0)$$

Diffusion from a boundary source (mechanisms 4, 5) or from dislocations (mechanism 6) is driven by a curvature difference

$$K_2 = \left(\frac{1}{\rho} - \frac{1}{x}\right). \qquad (3)$$

As x approaches a, K_2 starts to differ slightly from K_1. But experiments in which rows of spheres are sintered are rarely carried this far. For simplicity, we adopt
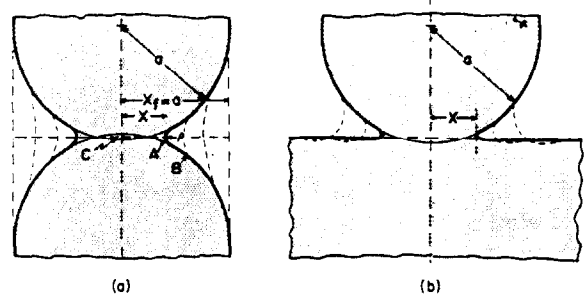

FIG. 3. The sintering of a row of spheres (a); or of a sphere to a plate (b). In both cases the curvature differences driving the various mechanisms decrease continuously.

a single curvature difference, K_1, as the driving force for all mechanisms during the sintering of a row of spheres, or of a sphere to a plate. The way in which K_1 varies with x/a is shown in Fig. 4(a).

Sintering of an aggregate of spheres. Of more practical interest—and complexity—is the driving force for the sintering of packed spheres. Figure 5 defines the problem. The upper part of the diagram shows the pore shape during stage 1; its smallest radius of curvature is ρ_1. Mechanisms which transport matter from one part of the pore to another (mechanisms 1–3 of Fig. 1) are driven by the differences
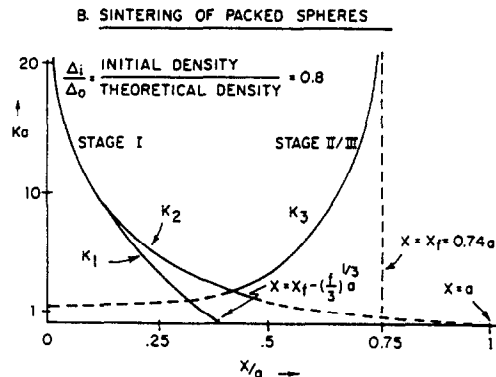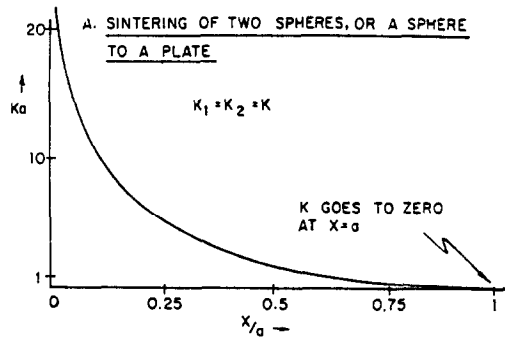

FIG. 4. (a) The curvature difference, K, driving the sintering of two spheres, or of a sphere to a plate; (b) the curvature differences driving sintering in a compact or aggregate of spheres.
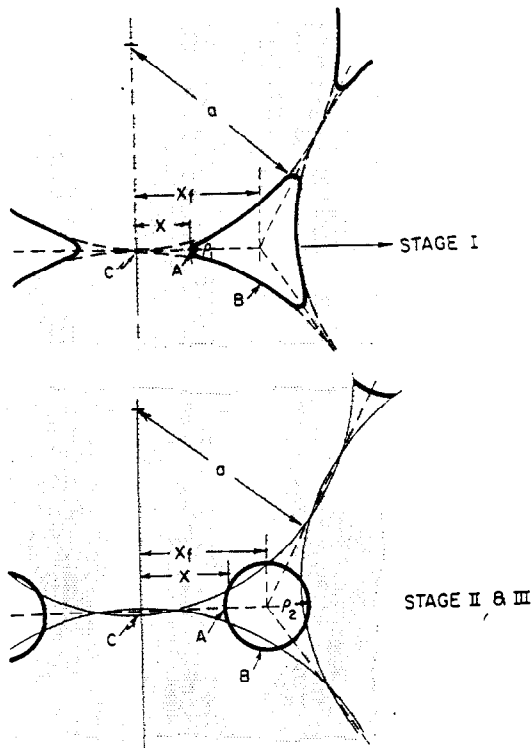
---

† The sintering of a sphere to a plate involves almost the same geometry. In this report we treat the two problems as identical.

‡ This choice is a compromise. If an equilibrium dihedral angle forms where the grain boundary between two spheres intersects the free surface, then sintering may stop before x grows to equal a. But in sintering a sphere to a plate, x may grow until it is larger than a. These extreme cases are seldom of interest because such model experiments are used to study the early stages of sintering only.

FIG. 5. The upper figure shows the geometry during stage 1 of sintering; the smallest radius of curvature is ρ_1. The lower one shows the assumed geometry during stages 2 and 3; the pores have become cylindrical or spherical with a radius of ρ_2.

in curvature around the pore itself: between points A and B in Fig. 5. When the neck size, x, is small, this curvature difference is

$$K = \frac{1}{\rho_1} - \frac{1}{x} + \frac{2}{a} \qquad (3)$$

(a curvature is negative when its center of curvature lies within the material; positive when it lies in the pore).

But the curvature difference must go to zero when the pore becomes cylindrical or spherical. If the initial density of the compact of particles is Δ_i, and the theoretical density of the material of which they are composed is Δ_0, then the volume fraction of space in the compact is

$$f = \frac{\Delta_0 - \Delta_i}{\Delta_0}.$$

If each pore sinters until it becomes spherical, and (on average) there are 3 pores per particle, then each spherical pore has a radius of $(f/3)^{1/3}a$. We therefore require that K_1 go to zero when (referring to Fig. 5):

$$x_f - x = \left(\frac{f}{3}\right)^{1/3} a$$

where x_f is the final value of x when 100 per cent density is reached.

This is achieved by modifying equation (3) as follows

$$K_1 = \left(\frac{1}{\rho_1} - \frac{1}{x} + \frac{2}{a}\right)\left(1 - \frac{x}{x_f - \left(\frac{f}{3}\right)^{1/3} a}\right) \qquad (4)$$

$$(K_1 \geq 0)$$

and, as before

$$\rho_1 = \frac{x^2}{2(a - x)}.$$

Mechanisms which transport matter from the grain boundary to the neck (mechanisms 4 and 5) are driven by the difference in curvature between points A and C (Fig. 5). This curvature difference does not go to zero when the pore becomes cylindrical or spherical. During stage 1, it is equal to $(+(1/\rho_1) - (1/x)]$. But when the pore becomes cylindrical or spherical (Fig. 5, stages 2 and 3) it becomes $1/\rho_2$ or $2/\rho_2$, respectively. We therefore adopt two expressions for the curvature driving mechanisms (4 and 5):

$$K_2 = \left(\frac{1}{\rho_1} - \frac{1}{x}\right) \quad \text{(stage 1)} \qquad (5)$$

$$K_3 = \frac{2}{\rho_2} \quad \text{(stage 2 and 3)} \qquad (6)$$

$$(K_2 \geq 0;\ K_3 \geq 0);$$

where $\rho_2 = x_f - x$ and $\rho_1 = [x^2/2(a - x)]$. (The justification for choosing the spherical pore-shape follows in Section 2.5).

The precise form of these curvatures is important. To give a clearer picture of how K_1, K_2 and K_3 (and thus the relative rates of the mechanisms) vary with neck size, they are illustrated schematically in Fig. 4(b) for a compact containing an initial volume fraction, f, or pores equal to 0.2. The reader may disagree with my choices, or feel (correctly) that they could be improved. They are compromises which emphasize simplicity and physical clarity rather than rigor, and they leave considerable scope for refinement. Such refinements can readily be incorporated into the computational scheme used to construct the diagrams.

For later reference we note that, for a two-dimensional compact of straight wires, packed as shown in Fig. 5,

$$x_f = 0.55a.$$

For a compact of spheres,

$$x_f = 0.74a$$

has been used.

2.3 Stage 0: Adhesion

When two particles are placed in contact, inter-atomic forces act between them, drawing them together. They deform elastically, forming a neck.[6] If they are absolutely clean (they rarely are, of course) an upper limit for the radius of this neck is

$$x \simeq \left(\frac{\gamma_{eff}}{a\mu}\right)^{1/3} a \qquad (7)$$

where γ_{eff}, an effective surface energy, is given by the *clean surface approximation*:

$$\gamma_{eff} \simeq 2\gamma_s - \gamma_B.$$

It is the change in free energy when two free surfaces are brought together to form a single grain boundary. (These forces contribute to the green strength of a compact. The neck thus formed is relatively large when the particle size is small: adhesion may play an important role in the behavior of sub-micron sized particles.)

Most particles are coated with an oxide, have an organic surface film, or are, in some other sense, dirty. Adhesion still occurs, but the forces involved are weaker. A lower limit is obtained by assuming them to be Van der Waals forces. The cohesive energy of a Van der Waals bonded solid is typically one twentieth as great as that of a metallic, ionic or co-valent solid (0.1 eV per atom instead of about 2 eV per atom). The lower limiting neck size is then given by equation (7), with γ_{eff} set equal to $\gamma_s/10$ (the *dirty surface approximation*).

It is at this stage that dislocation glide may contribute to sintering. The local stresses,[6] set up by the adhesion process, can be large—as large as the ideal shear strength. Experiments with bubble rafts[15]—which obey the clean surface approximation—show that dislocations are nucleated in the neck region, permitting some neck growth. With real materials this contribution to neck growth is comparable to that due to adhesion alone (equation 7), which we shall take as an adequate description of both.

To obtain a rate-equation, we assume that, when particles are placed in contact, interatomic forces draw them together at roughly the sound velocity ($c = 10^5$ cm/sec) until equilibrium is established at the neck size given by equation (7). This leads immediately to

$$(\dot{x})_0 = \frac{ca^2}{x} \quad \text{for} \quad x < \left(\frac{\gamma_s a^2}{10\mu}\right)^{1/3}$$

$$(\dot{x})_0 = 0 \quad \text{for} \quad x \geq \left(\frac{\gamma_s a^2}{10\mu}\right)^{1/3}. \qquad (8)$$

The diagrams of Sections 3 and 4 use the dirty surface approximation.

2.4 Stage 1: Diffusion controlled neck growth

At temperature above about $0.25\,T_M$, adhesion is followed by diffusion-controlled neck-growth. The diffusion quickly removes the contact-stresses generated during stage 0; from then on the diffusive fluxes are driven by difference in surface curvature (Fig. 1). The chemical potential of atoms at the neck where two particles meet is determined by the principal curvatures there. Matter flows into this region from all other parts of the system where the chemical potential is higher. The neck growth-rate is determined by the total flux of matter arriving at the neck; and this is simply the sum of the contributions from the several independent paths shown in Fig. 1. We now consider these in order. As before, we seek an equation for the instantaneous growth-rate in terms of the current geometry of the sample. All equations are derived by assuming a *quasi steady state* (concentration gradients reach steady values in a time which is short compared to that required for changes of geometry of the particles and neck); *equilibrium concentrations* at all sinks and sources; and all involve simplifying assumptions about the diffusion geometry and the magnitudes of chemical potential gradients.† All use the expression

$$V = 2\pi x \rho_1 \dot{x} \qquad (9)$$

to relate the volume flowing per unit time into the neck region (V) to the neck growth-rate, ($\dot{x}$), during stage 1 of sintering.

Surface diffusion from a surface source (mechanism 1) leads to an approximate rate of neck growth given by (Kuczynski,[5] Wilson and Shewmon[2]):

$$\dot{x}_1 = 2D_s\delta_s FK_1^3 \qquad (10)$$

where

$$F = \frac{\gamma_s \Omega}{kT}.$$

This equation is easily modified to include the contribution of *lattice diffusion from a surface source* (mechanism (2): Kuczynski,[5] Wilson and Shewmon[2]). The contribution is

$$\dot{x}_2 = 2D_v FK_1^2 \qquad (11)$$

Vapor transport from a surface source (mechanism 3: Kingery and Berg[10]) leads to a neck growth-rate

$$\dot{x}_3 = P_v F\left(\frac{\Omega}{2\pi\Delta_0 kT}\right)^{1/2} K_1. \qquad (12)$$

(This equation is appropriate for sintering in a vacuum—the case considered in this report. In an inert gas atmosphere vapor transport may be diffusion limited.)

Grain boundary transport from sources on the grain boundary (mechanism 4) is geometrically simpler than the others. Allowing the standard assumptions of a quasi steady-state, and equilibrium at sources and sinks, the diffusion problem can be solved exactly [see, e.g. Johnson[11]]. The result is:

$$\dot{x}_4 = \frac{4D_B \, \delta_B F K_2^{\,2}}{x} \tag{13}$$

a result which is misprinted in Ref. (2).

The problem of *lattice diffusion from sources on the grain boundary* (mechanism 5) has not been solved with similar rigor. An adequate result can be obtained by generalizing equation (13) to include the contribution from lattice diffusion, but there is disagreement about the appropriate way of doing this. I agree with, and have adopted, the approach of Wilson and Shewmon[2] which amounts to replacing the area across which the boundary flux flows, roughly $\pi x \delta_B$, by that across which the lattice diffusion flux passes, roughly πx^2; and replacing D_B by D_V. The contribution from lattice diffusion then becomes†

$$\dot{x}_5 = 4D_v F K_2^{\,2}. \tag{14}$$

These last two mechanisms translate particle centers together, causing densification.

Lattice diffusion from dislocation sources (mechanism 6) is a potential neck-growth mechanism. It has been argued that the surface stress induces a stress field within the neck region of order $\sigma = 2\gamma/x$, and that this drives dislocation creep. But steady creep is only possible if dislocations can be generated at sources—a process which requires that $\sigma > (\mu b/x)$, and hence (in the absence of applied stress) that $2\gamma > \mu b$. Since this inequality is never satisfied, steady-state creep by dislocation motion must be ruled out as a sintering mechanism—a conclusion reached by Wilson and Shewmon.[2]

Other possibilities remain. An attractive one is that all dislocation segments in the neck region climb, becoming curved, until they reach a configuration such that they are in static equilibrium. In climbing, the dislocations release matter which joins the neck. This *transient creep* contribution is discussed further in Appendix 1, where a rate equation is derived for it.

† *Note added in proof.* Recent unpublished calculations by G. Weatherly and D. Wilkinson indicate that this equation overestimates the contribution of lattice diffusion.

The result is

$$\dot{x}_6 = \tfrac{4}{9}K_2 N x^2 D_v F\left\{K_2 - \tfrac{3}{2}\frac{\mu x}{\gamma_s a}\right\}. \tag{15}$$

Of the various ways in which dislocations might contribute to sintering of an unstressed powder aggregate, this one appears to be the most important. But for reasonable values of the dislocation density, N, ($\leq 10^{12}$ cm/cm^3) even this contribution is negligible. Though included in the calculations described below, dislocation-dominated sintering rarely appears as a field on any of the diagrams simply because some other mechanism always goes faster. If external stresses are applied to the powder aggregate, of course, the situation changes: dislocations then may contribute in an important way to sintering.

Since they are all independent, the *net sintering rate* during stage 1 sintering is simply the sum of the six contributions listed in this section:

$$(\dot{x})_1 = \sum_{i=1}^{6} \dot{x}_i \tag{16}$$

2.5 Stages 2 and 3

As the neck grows, the curvature difference, which drives most of these mechanisms, slowly dwindles. For the calculations of this report, I have drawn a distinction between stage 1, when a driving force exists for redistribution of matter within a pore (from B to A in Fig. 5), and stages 2 and 3, when this driving force has largely disappeared. There remains a driving force for diffusive flow of matter from points on the grain boundary separating two particles (assuming that it is still there) and the pore: from C to A in Fig. 5. The subtler distinctions between stages 2 and 3 are ignored; instead they are treated as obeying the same set of rate equations.

Only two mechanisms are important: *boundary diffusion from sources on the boundary*, and *lattice diffusion from the same sources*. The first of these diffusion problems can be solved exactly—making the standard assumptions of a quasi steady-state, and perfect sinks and sources. The results for spherical and cylindrical pores are given in Appendix 2. They differ—though not enough to make important changes in the diagrams at the present level of approximation. Accordingly, we use the result for spherical pores, assumed to contain no internal gas pressure. The result is (equation B5):

$$\dot{x}_7 = \tfrac{1}{16}D_B \, \delta_B F K_3^{\,3}\left\{\frac{1}{\log_e\left(\dfrac{x_f K_3}{2}\right) - \dfrac{3}{4}}\right\}. \tag{17}$$

The problem of generalizing this to include a contribution from lattice diffusion is essentially the

same as that discussed in Section 2.4. We adopt the same solution, giving for the contribution of *lattice diffusion from boundary sources* the rate equation

$$\dot{x}_8 = \tfrac{1}{16} x D_v F K_3{}^3 \left\{ \frac{1}{\log_e \left(\dfrac{x_f K_3}{2} \right) - \dfrac{3}{4}} \right\}. \qquad (18)$$

The *net sintering rate* during stages 2 and 3 is given by

$$(\dot{x})_{2.3} = \dot{x}_7 + \dot{x}_8.$$

3. SINTERING DIAGRAMS

3.1 Construction and properties of the diagrams

Consider a two-dimensional space with neck-size and temperature as coordinates (Fig. 2). It is convenient to use as axes the *normalized neck-size* x/a and *homologous temperature* T/T_M, where T_M is the melting temperature of the material.

The construction of a diagram involves two stages. We first ask: *in what field of neck size/temperature*

TABLE 1

	Silver		Copper		Stoichiometric UO$_2$		Tungsten	
Atomic volume Ω (cm^3)	1.71×10^{-23}		1.18×10^{-23}		4.1×10^{-23}	(k)	1.59×10^{-23}	
Burgers vector b (cm)	2.98×10^{-8}		2.56×10^{-8}		3.86×10^{-8}		2.73×10^{-8}	
Melting point ($^\circ$K) T_M	1234		1356		3123		3683	
Shear modulus μ (dyn/cm^2)	2.64×10^{11}	(a, b)	4.21×10^{11}	(h, b)	8.3×10^{11}	(k, l)	1.55×10^{12}	(s)
Temp coeff of μ (/K)	4.36×10^{-4}	(a, b)	3.97×10^{-4}	(h, b)	1×10^{-4}	(k, l)	1.04×10^{-4}	(t)
Dislocation density	10^{10}		10^{10}		10^8		10^{10}	
Density (g/cm^3), Δ_0	10.5		8.96		10.94		19.3	
Surface energy γ_s (ergs/cm^2)	1120	(c)	1720	(c)	1000	(m)	2650	(c)
Eff. boundary thickness (cm)δ_d	5.78×10^{-8}		5.12×10^{-8}		5.54×10^{-8}		5.48×10^{-8}	
Eff. surface thickness (cm) δ_s	3.0×10^{-6}		3.0×10^{-8}		5.54×10^{-8}		3.0×10^{-8}	
D_0 for lattice diffusion (cm^2/sec)	4.4×10^{-1}	(d)	6.2×10^{-1}	(d)	6.8×10^{-5}	(n)	5.6	(u)
Activation energy for lattice diffusion Q_v kcal/mole	44.3	(d)	49.6	(d)	98.3	(n)	140.0	(u)
D_0 for boundary diffusion (cm^2/sec)	1.2×10^{-1}	(e)	10^{-1}		4×10^{-2}	(o)	10.0	(v)
Activation energy for boundary diffusion, Q_B (kcal/mole)	21.5	(e)	25.0	(†)	72.0	(o)	90.5	(v)
D_0 for surface diffusion (cm^2/sec)	5.0×10^7	(f)	2×10^4	(j)	3.4×10^5	(p)	8.5	(w)
Activation energy for surface diffusion, Q_s	63.6	(f)	49.0	(j)	108.0	(p)	78.0	(w)
Preexponential for vapor pressure, P_0 dyn/cm^2	9.53×10^{11}	(g)	1.23×10^{12}	(g)	4.11×10^{14}	(q, r)	3.23×10^{12}	(g)
Activation energy for evaporation, Q_{vap} kcal/mole	65.2	(g)	77.5	(g)	143.9	(q, r)	187.1	(g)

† Inferred by scaling data of materials of the same structure and of comparable melting points. The activation energy is the same as that observed for Au in Cu grain boundaries.[1]

(a) J. R. NEIGHBORS and G. A. AHLERS, *Phys. Rev.* 111, 707 (1958).

(b) Y. A. CHANG and L. HIMMEL, *J. appl. Phys.* 36, 3596 (1965).

(c) H. JONES, *Met. Sci. J.* 5, 15 (1971).

(d) N. L. PETERSON, *Solid State Phys.* 22, (1968).

(e) R. E. HOFFMAN and D. TURNBULL, *J. appl. Phys.* 22, 634 (1957).

(f) R. R. HOUGH, *Scripta Met.* 4, 559 (1970).

(g) S. DUSHMAN and J. M. LAFFERTY, Editors, *Scientific Foundations of Vacuum Technology.* Wiley (1962).

(h) W. C. OVERTON and J. GAFFNEY, *Phys. Rev.* 98, 969 (1955).

(i) A. E. AUSTIN, M. A. RICHARDS and E. WOOD, *J. appl. Phys.* 37, 3650 (1966).

(j) J. Y. CHOI and P. G. SHEWMON, *Trans AIME* 224, 589 (1962).

(k) P. J. BALDOCK, W. E. SPINDLER and T. W. BAKER, *J. Nucl. Mat.* 18, 305 (1966).

(l) J. B. WACHTMAN, M. L. WHEAT, H. J. ANDERSON and J. L. BATES, *J. Nucl. Mat.* 16, 39 (1965).
 P. SUNG and J. E. TURNBAUGH, *J. Nucl. Mat.* 24, 107 (1967).

(m) P. S. MAIYA, *Acta Met.* 19, 255 (1971).

(n) D. K. REIMANN and T. S. LUNDY, *J. Am. Ceram. Soc.* 52, 511 (1969).

(o) A. B. ALCOCK, R. J. HAWKINS, A. W. D. HILLS and P. McNAMARA, *Thermodynamics.* p. 57. I.A.E.A. (1966).

(p) P. S. MAIYA, *J. Nucl. Mat.* 40, 57 (1971).

(q) R. J. ACKERMANN, P. W. GILLES and R. J. THORN, *J. chem. Phys.* 25, 1089 (1956).

(r) M. TETENBAUM and P. D. HUNT, *J. Nucl. Mat.* 34, 86 (1970).

(s) H. B. HUNTINGTON, *Solid State Phys.* 7, 213 (1958).

(t) P. E. ARMSTRONG and H. L. BROWN, *Trans. AIME* 230, 962 (1964).

(u) Data of R. L. ANDELIN, J. D. KNIGHT and M. KAHN, *Trans. AIME* 233, 19 (1965) as modified by S. L. ROBINSON and O. D. SHERBY, *Acta Met.* 17, 109 (1969).

(v) K. G. KREIDER and G. BRUGGEMAN, *Trans. AIME* 239, 1222 (1967).

(w) B. C. ALLEN, *Trans. AIME* 236, 915(1966).

space is a given mechanism dominant—that is, where does it contribute more to the neck growth-rate than any other single mechanism? The *boundaries of these fields* are obtained by equating pairs of rate equations and solving for neck-size as a function of temperature. At field boundaries (shown as heavy lines on Fig. 2) two mechanisms contribute equally to the sintering rate. The heavy broken line marks the transition from stage 1 to stages 2 and 3: the mechanism does not change here, though the equation used to describe it does (Section 2). Above this line the rate of sintering increases with neck size: it might not do so if the pores contained trapped gas, but we have assumed they do not. On diagrams such as this one, which describe the sintering of an aggregate of particles, the fields in which a non-densifying mechanism is dominant are shaded.

Superimposed on the fields are *contours of constant neck growth-rate* (Fig. 2a), or of *constant time* (Fig. 2b). The neck growth-rate is the sum of the contributions due to each of the mechanisms listed in Section 2—with one restriction. Two rate-equations are listed for each of the two mechanisms (4 and 5): one pair is appropriate in stage 1, the other in stage 2/3. These pairs are treated as alternative, not additive, processes (for obvious reasons): the faster pair is added into the total rate; the slower pair is omitted from the sum.

Contours of constant time are computed by the same method—and with the same restriction—from an integral of the sum of the rate-equations with respect to time. No new physics is involved, but the resulting diagrams are usually more convenient to use; all but one of the figures in this report are of this second type. The diagrams are constructed by numerical computation. The data used to do this is listed in Table 1.

Figure 6 shows diagrams for aggregates of silver particles of two sizes: radii of 100 μm and 10 μm. (The temperature scale on this and most subsequent diagrams is expanded, and starts at $0.5T_M$.) Sintering at constant temperature is described by a vertical line on the diagram; more complicated time–temperature schedules can be plotted onto the diagram and show the dominant mechanism and neck-size, at each point in the schedule. Figure 6 illustrates that the relative size of a field depends on the particle size, a, because the rate-equations differ in their dependence on a. Obviously there is no single 'mechanism' of sintering: the mechanism which appears as dominant depends on temperature, on particle size, and on time: that is, on the stage that sintering has reached. The contours of constant time, too, are shifted if the
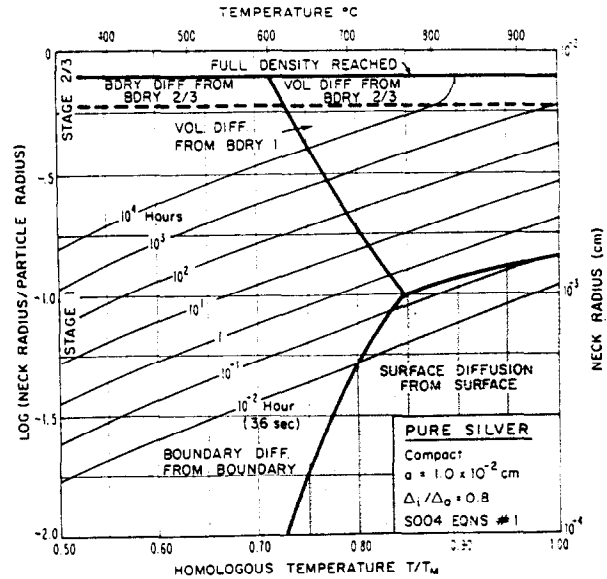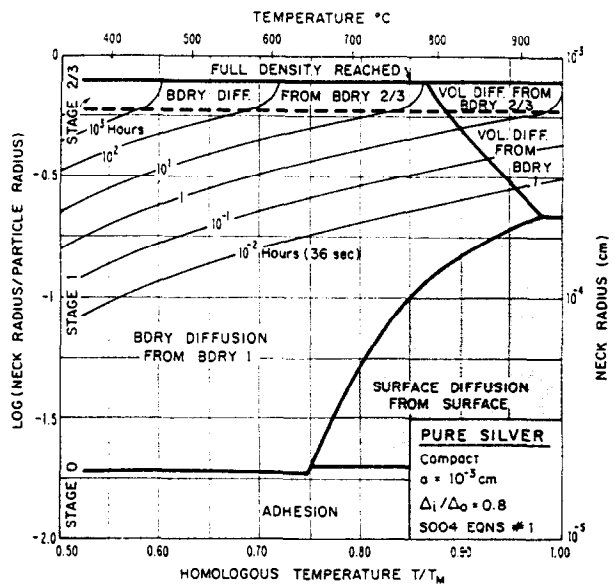
FIG. 6. (a) The sintering of an aggregate of silver spheres of radius $a = 100$ μm and initial relative density 0.8; (b) The same, for $a = 10$ μm spheres. Because the mechanisms depend on a in different ways, the field boundaries move when the particle size is changed. The time-contours also move: large particles sinter more slowly.

particle size changes, and may be moved from one field into another—as they are in Fig. 6.

Not all the mechanisms which contribute to sintering appear as fields. Vapor transport, for instance, is included in all the computations shown here, yet it does not appear as a field on Fig. 6. On Fig. 7, a diagram for the sintering of UO_2, it does—because the relative magnitudes of the vapor pressure and diffusion coefficients, etc. are different for UO_2 than for silver.
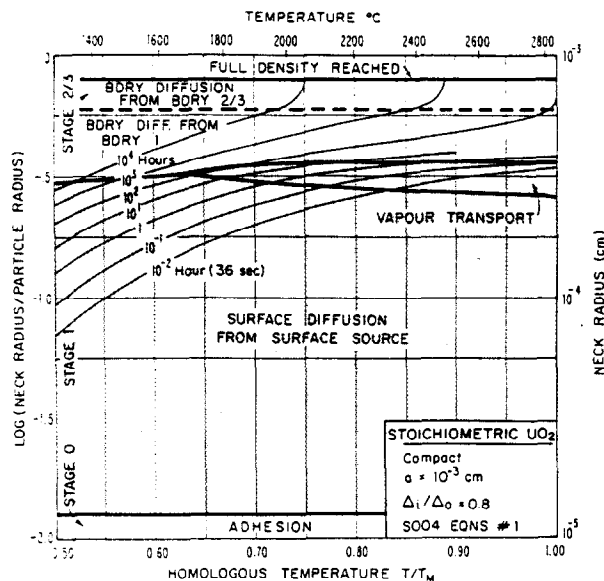
Change of microstructure drastically alters the

FIG. 7. A sintering diagram for an aggregate of UO$_2$ particles of radius 10 μm. Unlike the diagrams for tungsten and silver, vapor transport appears here as a dominant mechanism.
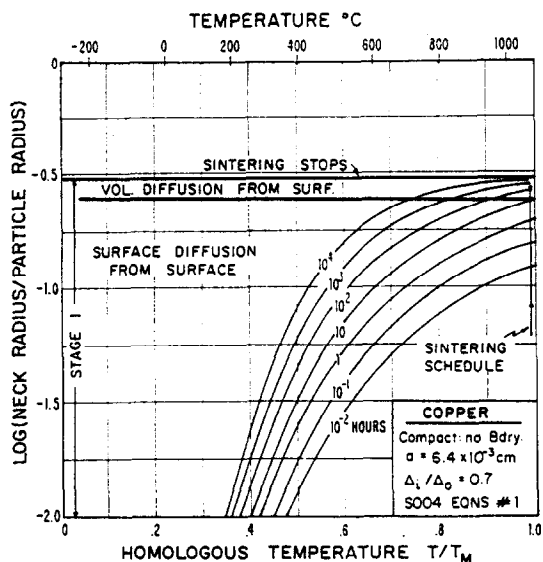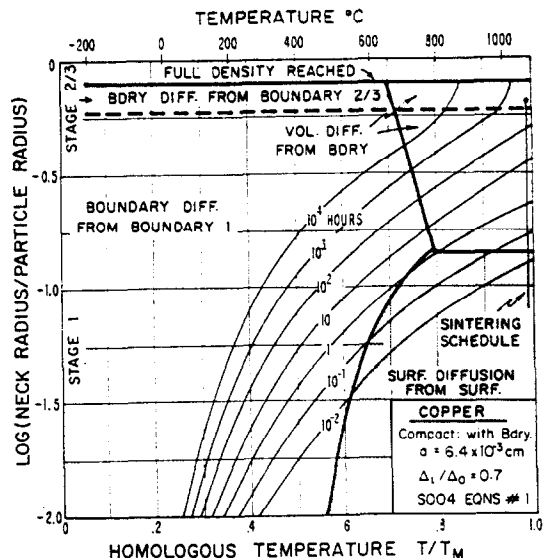

FIG. 8. The sintering of copper wires with, and without, a grain boundary in the neck between the wires. Removal of the boundary suppresses mechanisms which use it as a source. (The input data matches the experimental conditions of Alexander and Balluffi;[12] the diagrams should be compared with their Fig. 7.)

diagrams. Sintering near the melting point, for example, can cause grain growth or recrystallization. The neck between two particles then no longer contains a boundary, and mechanisms (4 and 5) (which use the boundary as a source) are suppressed. The result, for copper, is shown in Fig. 8: the rates of sintering are reduced, and neck growth stops completely when the neck size is about 0.32a; finally, a new field appears in which *volume diffusion from the surface* is dominant.

(The diagrams of Fig. 8 are designed to describe the experiments of Alexander and Balluffi,[12] who sintered copper wires ($a = 64$ μm) at 1075°C for 408 hr: their sintering schedule is shown as a vertical line on Fig. 8. This schedule caused grain growth and—as shown in their Fig. 7—necks with no boundary in them have grown to roughly the size predicted by Fig. 8b.)

3.2 *Limitations and extensions*

The diagrams are only as good as the equations and the data used to construct them. The equations listed in Section 2 are far from perfect: all are based on idealized geometries, and most make approximations in solving the diffusion equation. But the data is even less reliable. Grain boundary and surface diffusion coefficients are notoriously difficult to measure; where measurements exist, they are rarely reliable to better than a factor of 2. This is not a defect of the diagrams themselves—it simply reflects

the state of our understanding of sintering and of the parameters which determine its rate.

For certain mechanisms, more precise rate-equations exist, or could be developed. But until data improves, it appears more rewarding to extend the diagrams to include such things as the effect of internal gas pressure, external pressure or stress, interface-reaction controlled kinetics, grain growth during sintering, and activated sintering. The computational scheme described above is a very flexible one: all these phenomena can readily be included in it.

4. APPLICATIONS

The final section of this report illustrates the application of the diagrams to the interpretation of experiment, and to the design of sintering schedules.

4.1 The design and analysis of experiment

(a) *Kuczynski's measurements on copper.* Kuczynski,[5] in a classic study of sintering, measured the neck growth-rate of copper spheres ($a = 40 \ \mu$m) on a copper plate. The ranges of temperature and time he used, and the resulting range of neck size, was

$$T = 700–900°C$$

$$t = 0.5–41 \ \text{hr}$$

$$\frac{x}{a} = 0.1–0.31.$$

Figure 9 shows the appropriate diagram. (It was computed by using rate equations (8–16) inclusive, and setting K_1 and K_2 both equal to equation (2).) The box on the diagram is bounded by the ranges of T and t that Kuczynski used. The neck size is predicted tolerably well: comparing predictions for a given T and t with experiment shows a maximum discrepancy of 20 per cent in x/a. For most data points, the agreement is much closer: typically 5 per cent error.
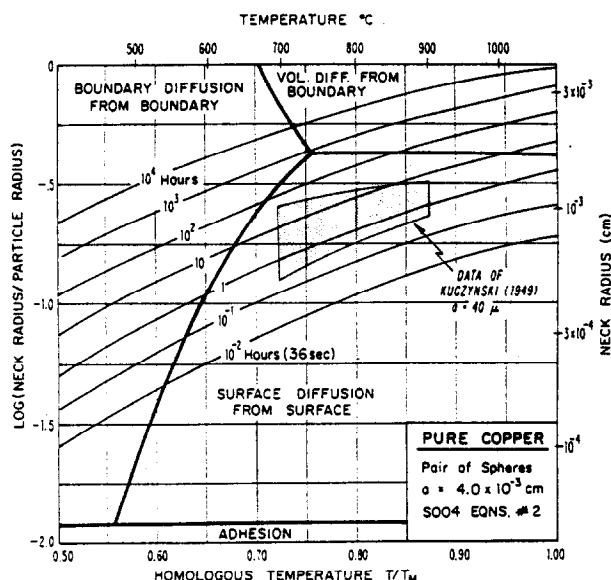

FIG. 9. This diagram describes the sintering of a copper sphere to a plate. With this geometry the driving force decreases continuously (as explained in Section 2.2) and the mechanisms corresponding to stages 2 and 3 are absent. The shaded box shows the range of time and temperature investigated by Kuczynski.[5]

The data lies entirely in the field for which *surface diffusion from a surface source* is dominant, though the low temperature end is close enough to the boundary diffusion controlled field so that the contribution from it—and from volume diffusion—will be appreciable.

Kuczynski interpreted the data as indicating volume diffusion control. His conclusion was based on the determination of the exponent,† n, in the equation

$$x^n = At,$$

and on an experimental activation energy close to that for lattice self-diffusion.

This apparently attractive method of matching a mechanism to the exponent, n, is misleading for two reasons. First, the sintering rate is rarely determined by a single mechanism: it is usually the sum of several contributions, with relative magnitudes that change as sintering proceeds. (At a field boundary, two mechanisms contribute equally; where three fields meet, three do.) This alone makes deductions based on n unsure; they become even less certain when the detailed geometry of a single mechanism is considered (Nichols[4,8]). Then it is found that a mechanism is not characterized by a constant, integer value of n, as the simple equations (10–14) would predict.

An activation energy does characterize a mechanism, provided it acts alone. But the reported activation energies for surface and volume diffusion in copper are almost identical: 49.0 and 49.6 kcal/mole. Our conclusion (fully supporting that first reached by Wilson and Shewmon[2]) is that surface diffusion was dominant in Kuczynski's experiments on copper. The exponent, n, and the activation energy are not usually sufficient to identify the dominant mechanism of sintering, though an experiment conducted in the center of a field, far from all field boundaries, might give useful data. But although I believe the diagram method is a better way of interpreting experiments, its conclusions should be treated cautiously for the reasons given in Section 3.2; different input data could lead to different conclusions.

(b) *Kuczynski's measurements on silver.* Similar experiments[5] on silver ($a = 180 \ \mu$m) are reanalyzed in Fig. 10. (This diagram was constructed from the equations, and with the curvature listed under 4.1(a). Note that a vapor transport field appears.) The

---

† If equations (10–14) are integrated with respect to time, a set of equations of this form is obtained. The exponent, n, characterizes a mechanism.
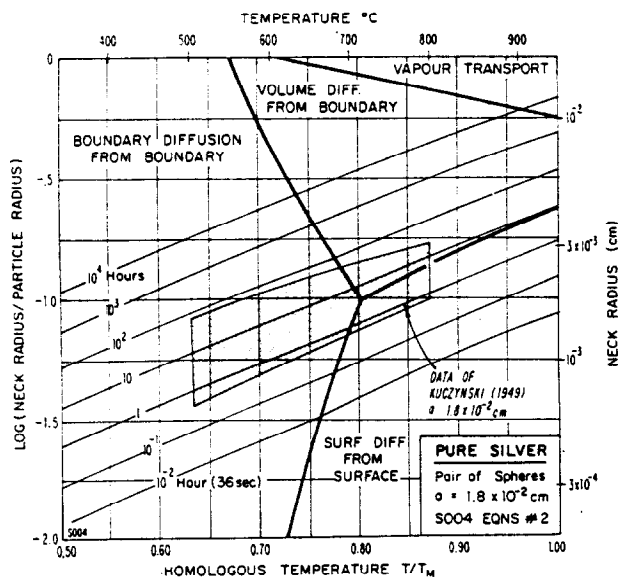
FIG. 10. The sintering of 180 μ silver spheres to a plate. The shaded box indicates the range of time and temperature investigated by Kuczynski.[5] His investigation overlaps three fields.

data spans the ranges

$$T = 500–800°C$$

$$t = 1–90 \text{ hr}$$

$$\frac{x}{a} = 0.033–0.162.$$

The shaded region is bounded by the ranges of T and t that Kuczynski used. The maximum error in predicting x/a is 12 per cent (and is systematic: it appears to indicate that the rate of grain-boundary diffusion is overestimated on the diagram).

The data overlaps three fields: it is an example of just how complicated the interpretation of sintering can be, even in model experiments like this one. More of the data lies in the boundary-diffusion-controlled field than in any other; but throughout the range of these experiments, boundary, volume and surface diffusion contribute significantly to neck growth. Clearly it is hopeless to rely on the exponent, n, or an activation energy, to identify 'the mechanism': both vary continuously over this range of T and t. (With the insight the diagram gives, one looks for a different trend than did Kuczynski: a high activation energy where volume and surface transport dominate, and a lower one where boundary diffusion takes over. In fact the data can be re-analyzed in this framework to give an activation energy of 57 kcals at the higher temperatures, and of 28 kcals at the lower ones.)

Our conclusion is that the data are consistent with, and logically explained by, a dominance of grain-boundary diffusion below 700°C, and a superposition of volume and surface diffusion above.

(c) *The measurements of Kingery and Berg on copper.* Kingery and Berg[10] measured neck growth between two spheres of copper ($a = 57\mu$m). Their ranges of T and t limit the box shown on Fig. 11 (the diagram was constructed as described in 4.1.a). The predicted neck sizes are in broad agreement ($\pm 20\%$) with those observed.

By measuring the exponent, n, and the activation energy, the authors concluded that volume diffusion was the dominant mechanism. Reasons for mistrusting conclusions based on these two measurements were listed in Section 4.1(a), and seem to apply here: the diagram indicates surface diffusion.

Our conclusion is that surface diffusion is dominant, with a significant contribution from volume diffusion.

(d) *The measurements of Wilson and Shewmon on copper.* Wilson and Shewmon[2] measured neck growth in a row of copper spheres. Some of their data (that for $a = 88$ μm) is shown on Fig. 12. The diagram supports their conclusion that surface diffusion is generally dominant, though it also indicates a large contribution from volume diffusion, which may become the dominant mechanism at the larger neck sizes. It is obviously *not* correct to state that surface diffusion always dominates neck growth: above a certain neck size ($x/a = 0.32$ in this case) volume diffusion takes over, and below a certain temperature
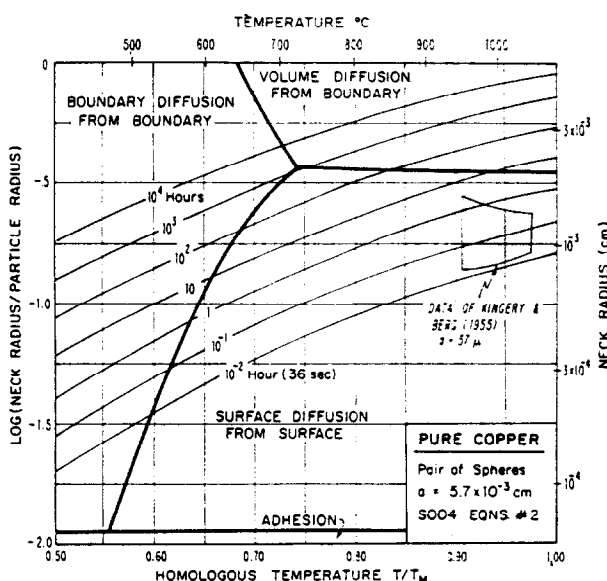

FIG. 11. The sintering of two copper spheres of radius 57 μm The shaded box shows the region investigated by Kingery and Berg.[10] It lies entirely in the surface-diffusion controlled field.
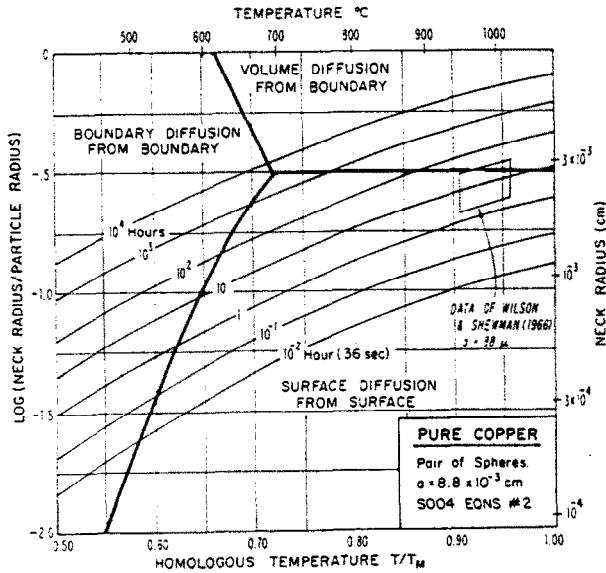
FIG. 12. The sintering of two copper spheres of radius 88 μ. The box shows the area investigated by Wilson and Shewmon[2] for this particle size.

(0.55 T_M in this case) grain boundary diffusion dominates at all neck sizes.

It may not be sufficiently appreciated that the sintering of a *row* of spheres and of a *compact* of spheres may differ in mechanism. Suppose, for instance, that a *compact* of copper spheres of the same size (88 μ) as those used by Wilson and Shewmon, was sintered for the same times and temperatures. The appropriate diagram is shown in Fig. 13: the box
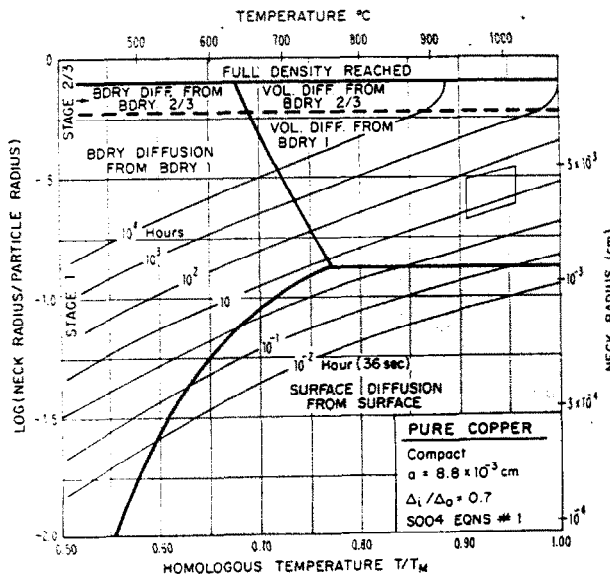

FIG. 13. The sintering diagram for an *aggregate* of spheres of the same size as those of Fig. 12. Because the geometry of the neck between two isolated spheres differs from that in a compact, the fields differ in size and position. The box of Fig. 12, if plotted onto this diagram as shown, now lies entirely in a volume-diffusion limited field.

now lies entirely in the volume-diffusion limited field The reason is contained in Fig. 4. Because of the geometry of a compact, the driving force for surface diffusion (K in Fig. 4a; K_1 in Fig. 4b) goes to zero at a smaller value of x/a in the compact. This does not mean that sintering stops—merely that another mechanism (in this case, volume diffusion from the grain boundary) takes over.

(e) *The measurements of Seidel and Johnson on silver.* As an example of the sintering of a compact, Fig. 14 shows the data of Seidel and Johnson[13] for silver ($a = 38 \mu$). Data for T and x/a (but not t) are given in their paper and were used to construct the shaded box. In agreement with these authors' own conclusions, the diagram suggests that volume
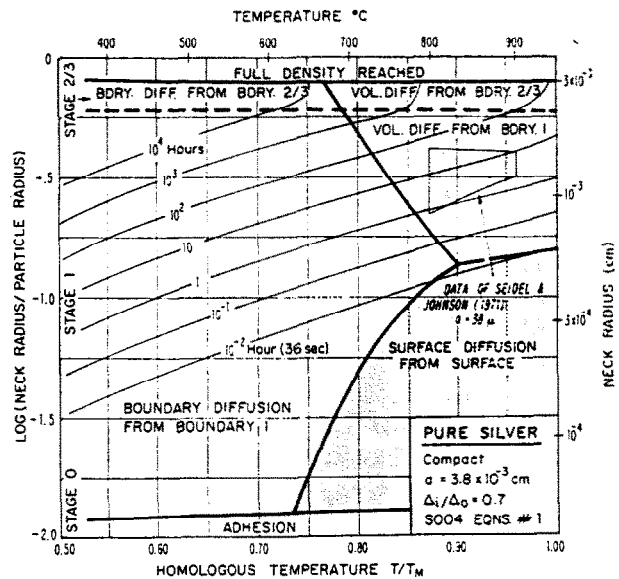

FIG. 14. The sintering of an aggregate of spheres of radius 38 μ. The initial relative density is 0.7. The box shows the area investigated by Seidel and Johnson.[13] It lies in the volume diffusion controlled field.

diffusion is dominant, and that boundary diffusion is the next important contributor. Surface diffusion contributes relatively little in this case. But no generalizations can be made: under other conditions (smaller a; shorter times; lower temperatures) other mechanisms would dominate.

4.2 Sintering schedules

The diagrams allow sintering schedules to be visualized and compared. Figure 8 showed a simple example. Another is shown in Fig. 15, which describes the sintering of UO$_2$ with a particle size of 2 μ ($a = 1 \mu$).

The short holds at 800 and 1500°C are designed to give strength to the compact to minimize fracture during subsequent heating. Even at these low
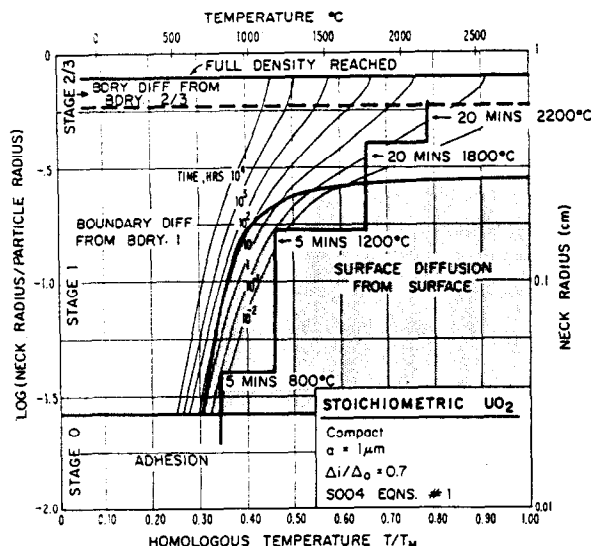
Fig. 15. The sintering of a compact of UO_2 ($a = 1$ μ). The initial relative density is 0..7 (The vapor transport field of Fig. 7 does not appear here because of the different particle size.) A hypothetical sintering schedule to produce porous UO_2 is shown. Other schedules are readily visualized with the help of the diagram.

temperatures (0.34 T_M and 0.47 T_M) some neck growth occurs—in this case by surface diffusion. This is followed by 20 min at 1800°C and 20 min at 2200°C. During these two steps, boundary diffusion from the grain boundary is dominant. (Here we have assumed that every neck contained a boundary; if grain growth occurred during this treatment, the diagram would be altered in the way shown by Fig. 8. For a dense product, grain growth must be suppressed.) The schedule ends on the line which separates stage 1 from stage 2: at this point all pores are cylindrical or spherical.

Alternative schedules leading to the same final neck size are readily visualized. Paths that allow a large contribution from surface diffusion tend to lead to a low density. Those that avoid shaded fields tend to give a higher density (at the same neck size).

For practical reasons, production schedules seldom involve times of more than a few hours. But sintering may continue in service. Figure 15 shows that sintering and densification will continue in this UO_2 compact at 1000°C when times of 10^4 hr or more are available—even in the absence of an external pressure.

5. SUMMARY

(1) The paper presents an attempt to synthesize the result of sintering models into useful diagrams. The diagrams can be used to display the sintering behavior of a specific material; as an aid to the design and interpretation of experiment; and as a

way of visualizing commercial sintering schedules and the effects of changes in schedule.

Six or more distinguishable mechanisms contribute to sintering (in the absence of applied stress). The diagrams identify, at a given temperature, particle size and neck size, the dominant mechanism, and show the rate of sintering that all the mechanisms, acting together, produce.

(3) Their use is illustrated by applying them to the experimental measurements of Kuczynski,[5] Kingery and Berg,[10] Wilson and Shewmon[2] and Seidel and Johnson,[13] and to the display of sintering schedules.

(4) The computational scheme used to construct such diagrams is a flexible one which allows the inclusion of grain growth, pore dragging, and externally applied pressure or stress—provided their effect on the rate of neck growth is known.

REFERENCES

1. F. THUMMLER and W. THOMMA, Met. Rev. 115, 69 (1969).
2. T. L. WILSON and P. G. SHEWMON, Trans. AIME 236, 48 (1966).
3. R. L. COBLE, J. Am. Ceram. Soc. 41, 55 (1958).
4. F. A. NICHOLS, J. appl. Phys. 37, 2805 (1966); Acta Met. 16, 103 (1968).
5. G. C. KUCZYNSKI, Trans. AIME 185, 169 (1949).
6. K. E. EASTERLING and A. R. THOLEN, Physics of Sintering (special issue) p. 77 (1971); Met. Sci. J. 4, 130 (1970); Acta Met. 20, 1001 (1972).
7. M. F. ASHBY, Scripta Met. 3, 837 (1969); Surface Sci. 31, 498 (1972).
8. F. A. NICHOLS and W. W. MULLINS, Trans. AIME 233, 1840 (1965).
9. J. G. R. ROCKLAND, Acta Met. 14, 1273 (1966).
10. W. D. KINGERY and M. BERG, J. appl. Phys. 26, 1205 (1955).
11. D. L. JOHNSON, J. appl. Phys. 40, 192 (1969).
12. B. H. ALEXANDER and R. W. BALLUFFI, Acta Met. 5, 666 (1957).
13. B. R. SEIDEL and D. L. JOHNSON, Physics of Sintering 3, 143 (1971).
14. J. P. HIRTH and J. LOTHE, Theory of Dislocations. McGraw-Hill (1968).
15. F. V. LENEL, G. S. ANSELL and R. C. MORRIS, Advanced Experimental Techniques in Powder Metallurgy, p. 61. Plenum (1970); Modern Developments in Powder Metallurgy, edited by H. HAUSNER, Vol. 4, p. 199. Plenum (1971).

APPENDIX 1: DISLOCATION INDUCED SINTERING

Consider a Frank net of dislocations of density N/cm² in the neck region. The average segment length, $l \simeq N^{-1/2}$. These segments act as sources for matter, climbing between nodes of the net which act as pinning points, until their curvature prevents

further climb. The climb force per unit length on a segment at any instant is

$$\left(\frac{\gamma_s b}{\rho} - \frac{\mu b^2}{R}\right)$$

where ρ is its current radius of curvature of the neck, and R that of the dislocation. The first term is the chemical force due to the increased chemical potential of atoms caused by the neck curvature; the second is the restoring force due to dislocation curvature. Using a standard expression (Hirth and Lothe,[14] equation 15–91) we obtain the dislocation climb velocity

$$v_{\text{dis}} = \frac{D_v \Omega}{bkT}\left(\frac{\gamma_s}{\rho} - \frac{\mu b}{R}\right). \tag{A1}$$

As a segment climbs it releases matter at a rate $2/3 lb v_{\text{dis}}$. If n segments contribute, matter flows into the neck region at a rate

$$\dot{V} = \tfrac{2}{3}nblv_{\text{dis}}. \tag{A2}$$

Using the standard relation, $\dot{V} = 2\pi x\rho\dot{x}$, we obtain the neck growth rate:

$$\dot{x} = \frac{nl}{3\pi x\rho}\, D_v F\left\{\frac{1}{\rho} - \frac{\mu b}{\gamma_s R}\right\}. \tag{A3}$$

The segments which contribute to neck growth are those contained in the neck region. Approximating its volume by $\tfrac{4}{3}\pi x^3$, we obtain

$$n = \frac{4\pi x^3 N}{3l}.$$

Finally, we note that, if the neck grows by this mechanism alone, the current neck radius, x, is related to the radius of curvature, R, of the dislocation segments. In climbing to a radius, R, each segment releases a volume, $(l^3 b/8R)$, of matter. The total volume which has entered the neck is

$$V = \frac{nl^3 b}{8R} = \frac{\pi x^4}{4a}.$$

If the resulting equation, $R = (2ab/3x)$, is substituted into equation (A3), we obtain

$$\dot{x} = \frac{4}{9}\frac{Nx^2 D_v F}{\rho}\left\{\frac{1}{\rho} - \frac{3}{2}\frac{\mu x}{\gamma_s a}\right\} \tag{A4}$$

I have investigated the circumstances under which this contribution to sintering becomes dominant. If the dislocation density, N, and the particle radius, a, are sufficiently large ($N \geq 10^{12}$ cm/cm^3; $a \geq 1$ mm), this mechanism appears as a narrow field on the diagrams, meaning that it dominates over a narrow range of temperature and neck size; such high dislocation densities are uncommon, though conceivable. The range of dominance appears in the early stages of sintering, and does not contribute in an important way to densification. It would appear that dislocations do not contribute in any important way to sintering in the *absence* of an applied stress or pressure—though their effects will obviously be important when stress or pressure is applied.

APPENDIX 2: THE SINTERING OF SPHERICAL AND CYLINDRICAL PORES BY BOUNDARY DIFFUSION

In this Appendix we derive, by standard methods, and in a form appropriate to the scheme of this paper, rate-equations for the shrinkage of spherical pores and of cylindrical pores with the cylinder axis lying in the boundary plane.

Consider a periodic array of spherical pores on a grain boundary. The nearest neighbor pore separation is $2x_f = 2a/\sqrt{3}$ (Fig. 5b). We attribute a circle of influence of radius x_f to each pore, and assume it contains no internal gas pressure. If a quasi steady-state is established, the divergence of the boundary flux, J_B, is constant, that is

$$\nabla \cdot J_B = -\frac{D_B}{\Omega kT}\nabla^2\mu = \text{constant} \tag{B1}$$

giving the field equation

$$\nabla^2\mu = C \tag{B2}$$

where μ is the chemical potential of the diffusing species. The solution is:

$$\mu = A\ln r + B + \frac{Cr^2}{4} \tag{B3}$$

where r is a radial distance from the pore center in the boundary plane. The boundary conditions are

(1) $J_B = 0$ at $r = x_f$ by symmetry

(2) $\mu = \dfrac{2\gamma_s\Omega}{\rho_2}$ at $r = \rho_2$ \hfill (B4)

(3) $\displaystyle\int_{\rho_2}^{x_f} 2\pi r\mu\, dr = 2\pi\rho_2\gamma_s\Omega$

the last condition being a statement of equilibrium.

Applying the boundary conditions and neglecting terms of order ρ_2/a and $(\rho_2/a)^2$ compared with unity, we obtain

$$\dot{x} = \tfrac{1}{16}D_B\delta_B F K_3^3\left\{\frac{1}{\log_e\left[\frac{x_f K_3}{2}\right] - \frac{3}{4}}\right\} \tag{B5}$$

for spherical pores, where $K_3 = 2/\rho_2$. If, instead, a periodic array of parallel cylindrical pores is assumed (the cylinder axis lying in the grain-boundary plane), the result is

$$\dot{x} = \frac{3}{2\pi}\left\{\frac{D_B\,\delta_B F K_3^2}{x}\right\} \tag{B6}$$

where, for cylindrical pores, $K_3 = 1/\rho_2$.